

Adaptive Resource Allocation Utilizing Periodic Traffic and Clock Drift in LPWAN

Aoto Kaburaki¹, Graduate Student Member, IEEE, Koichi Adachi², Senior Member, IEEE, Osamu Takyu³, Member, IEEE, Mai Ohta, Member, IEEE, and Takeo Fujii⁴, Senior Member, IEEE

Abstract—Low-power wide area networks (LPWANs), such as long-range wide area networks, are increasingly adopted as a communication standard for wireless sensor networks. LPWAN has been adopted for systems that periodically collect data from sensors, such as in environmental monitoring. However, continuous packet collisions may occur in periodic traffic systems owing to the adoption of a simple random-access scheme in LPWAN. In addition, the use of low-cost nodes results in clock drift, rendering the synchronization of nodes in the system challenging. Thus, this study proposes a wireless resource allocation scheme to avoid continuous packet collisions under the adverse effect of such clock drift. In the proposed scheme, the gateway determines the transmission offset and frequency channel for each node utilizing the periodic traffic feature and clock drift. Based on computer simulation results, the proposed scheme can improve the packet delivery rate by over 20% compared with benchmark methods.

Index Terms—Internet of Things (IoT), LoRaWAN, low-power wide area networks (LPWAN), resource allocation.

I. INTRODUCTION

THE Internet-of-things (IoT) in which various devices connect to the Internet, has become increasingly significant in various applications owing to the smaller size and lower energy consumption of wireless devices [1]. In a wireless sensor network (WSN), an IoT application aims to collect environmental information, such as temperature and CO₂ from sensors. Consequently, low-power wide area networks (LPWANs) are attracting attention because they can realize a long-distance communication of up to several kilometers at low cost [2], [3], [4], [5], [6], [7].

Primarily, LPWAN standards are classified into licensed and unlicensed systems. Licensed LPWANs include long-term evolution-machine and narrowband IoT, which are based on

developed cellular technologies that utilize licensed frequency bands; hence, they can achieve high data rates [8]. Conversely, unlicensed LPWANs, such as LoRaWAN and Sigfox, utilize unlicensed frequency bands and inexpensive nodes; hence, they are highly scalable at low cost. LoRaWAN is a widely used unlicensed LPWAN technology owing to its flexibility and scalability [8], [9].

Duty cycle (DC) is essential in realizing spectrum sharing among the various systems in the unlicensed bands. DC determines the ratio of the time in which a transmitter can access a particular frequency channel during a particular period.

Because LPWAN nodes are inexpensive, their circuit configuration is generally of low quality and cost [5]. In particular, their clock is inaccurate. Generally, LPWAN nodes use cheap crystal oscillators for internal clocks, whose accuracy is influenced by various physical factors, such as temperature and aging. Thus, unintentional changes in the one-clock value may occur [10]. Thus, a time shift called *clock drift* accumulates over time between a transmitting and receiving node [11], [12], [13], [14]. Suppose the LPWAN adopts a centralized time-domain resource allocation, such as time division multiple access (TDMA). In that case, clock drift must be compensated for to maintain strict synchronization among nodes and gateway (GW). This can be resolved by periodically transmitting a beacon signal from a GW to all nodes. However, synchronization becomes more challenging with increasing LPWAN nodes because LPWAN nodes are limited in the timing available to receive the downlink (DL) signal. Therefore, enabling all nodes to listen to broadcast beacons for synchronization is challenging. In addition, transmitting a node-specific synchronization signal to all nodes is challenging owing to the DC limitations of the GW. Furthermore, clock drift occurs when beacons are transmitted for synchronization, resulting in unintended changes in transmission timing and packet collisions.

Generally, in industrial applications, such as smart cities and smart agriculture, WSNs placed in a particular area monitor the environment and periodically transmit sensing data to an information aggregation station, such as a GW. LPWAN adopts an asynchronous random-access protocol, such as the pure ALOHA protocol for the medium access control (MAC) layer to reduce the cost and power consumed by sensor nodes. In the pure ALOHA protocol, a sensor node transmits a packet immediately after generating the packet. Thus, multiple sensor nodes may simultaneously transmit packets on the same wireless resource, resulting in packet

Manuscript received 5 December 2022; revised 24 May 2023; accepted 20 August 2023. Date of publication 11 September 2023; date of current version 11 April 2024. This work was supported by the research project under Grant MIC/SCOPE JP205004001. The associate editor coordinating the review of this article and approving it for publication was J. Liu. (Corresponding author: Aoto Kaburaki.)

Aoto Kaburaki, Koichi Adachi, and Takeo Fujii are with the Advanced Wireless and Communication Research Center (AWCC), The University of Electro-Communications, Chofu, Tokyo 182-8585, Japan (e-mail: kaburaki@awcc.uec.ac.jp).

Osamu Takyu is with the Department of Electrical and Computer Engineering, Faculty of Engineering, Shinshu University, Nagano 380-8553, Japan.

Mai Ohta is with the Department of Electronics Engineering and Computer Science, Faculty of Engineering, Fukuoka University, Fukuoka 814-018, Japan.

Color versions of one or more figures in this article are available at <https://doi.org/10.1109/TWC.2023.3311679>.

Digital Object Identifier 10.1109/TWC.2023.3311679

1536-1276 © 2023 IEEE. Personal use is permitted, but republication/redistribution requires IEEE permission. See <https://www.ieee.org/publications/rights/index.html> for more information.

collision at the receiving node. A carrier sense (CS)-based random-access protocol was proposed for LPWAN to reduce the number of packet collisions [15]. The CS does not require synchronization between sensor nodes. However, because sensor nodes are distributed within a vast area in LPWAN, a hidden node problem occurs, and packet collision may frequently occur [16].

Frequent packet collisions occur in LPWANs owing to the simple MAC layer access protocols. In addition, the traffic type of LPWAN significantly influences the occurrence of packet collisions. The LPWAN traffic is dominated by periodic uplink (UL) traffic, which differs from the random and high data rate traffic in conventional cellular communication and Wi-Fi systems [17], [18], [19], [20]. First, UL-dominated traffic provokes packet collisions, resulting in packet reception failure at the GW. The packet collision probability increases with an increase in the number of sensor nodes [18]. Second, periodic traffic includes continuous packet collisions between particular sensor nodes [21]. Continuous packet collisions severely degrade information updates at the GW, such as age-of-information (AoI) [22], [23]. The interval of information update at the GW is an essential indicator for communication quality in recent years [23], [24], [25]. When a packet collision occurs, a sensor node cannot immediately retransmit the packet due to the DC constraint. Consequently, retransmissions in LPWAN increase the channel occupation time of each sensor node and result in severe delays. Therefore, because LPWAN must deliver data to the GW with a single packet transmission, packet collision avoidance technology that considers LPWAN traffic is urgently required.

A. Related Studies

Packet collision in WSN can be avoided by radio resource allocation [15], [19], [21], [26], [27], [28]. Two main types of radio resource allocation exist, centralized and decentralized type. In the centralized type, a control station allocates radio resources to all the nodes in the system via DL packets, including control information. However, each node autonomously determines the radio resource to be accessed in the decentralized radio resource allocation. Generally, the centralized type outperforms the decentralized type; however, the centralized type must transmit control signals, resulting in overhead.

1) *Centralized Resource Allocation*: A transmission scheduling scheme was proposed for multi-hop sensor networks with periodic traffic in the IEEE 802.11 environment [21]. The scheme accommodated multiple nodes that periodically transmit packets. Continuous packet collision can be avoided by scheduling the transmission timing of nodes without stringent synchronization between nodes. However, overhead is inevitable because the scheduling scheme must transmit control information to all the nodes. In addition, frequency channel allocation is not considered.

In [26], we proposed a centralized radio resource allocation scheme for periodic traffic WSNs. This scheme aims to avoid packet collisions; the GW schedules the frequency channel and transmission timing for each node. However, the scheduling may not work efficiently with common sensor nodes owing

to unexpected changes in transmission timing with clock drift [11].

We propose a centralized radio resource allocation scheme that avoids packet collisions in periodic traffic in LPWANs, considering the characteristics of the periodical traffic.

Reference [19] proposed an adaptive MAC scheduling scheme called SMAC for periodic UL communication in LoRaWAN. In SMAC, a unique parameter of LoRaWAN, spreading factor (SF), was used for scheduling, such that the transmission timing and frequency channel do not overlap between nodes with the same SF. Broadcast beacons are used to establish synchronization between nodes for scheduling in SMAC. However, LPWAN nodes, such as LoRaWAN class A nodes, can receive a downlink signal for a limited duration only. Thus, sending such a broadcast beacon to the nodes within the system may be challenging. Furthermore, signals with different SFs are assumed to be orthogonal.

Reference [27] proposed a near-optimal frequency channel and power allocation scheme based on matching theory. A joint optimization problem of the channel and power allocation was formulated to achieve fair throughput among nodes. A matching-theoretic algorithm was used to achieve near-optimal frequency channel allocation because this optimization problem was NP-hard. However, because the scheme was evaluated for relatively fewer nodes, its scalability remains unclear.

An SF and transmit power allocation method is proposed using machine learning [29]. Two independent learning models were used to obtain the appropriate SF and transmit power for a node to minimize its energy consumption while maximizing the packet reception ratio. Considering the computational load on the nodes, the transmit power allocation was performed in a centralized approach, whereas each node performed the SF allocation in a decentralized approach. However, the mechanism of how the transmit power calculated by the centralized approach is fed to each node was not mentioned.

From the aforementioned analysis, conventional centralized resource allocation methods are designed on the premise of synchronization. Thus, in a completely asynchronous environment, the conventional centralized resource allocation methods may have performance limitations. In addition, owing to the DC constraints and received windows of the nodes, applying [19], [21], [27] when large numbers of nodes exist is challenging.

2) *Autonomous Decentralized Control*: As an autonomous decentralized type, listen-before-talk (LBT) protocols, such as carrier sense multiple access/collision avoidance (CSMA), are adopted for LPWAN [15], [30]. Each node listens to the frequency channel's status on which it will transmit a packet when using the LBT protocol. The node transmits the packet when the frequency channel is free, reducing the packet collision probability. CSMA-x is proposed as an LBT scheme for LoRaWAN [30]. CSMA-x simplifies the operation of CSMA/CA such that it can be introduced to LoRaWAN. In CSMA-x, a node listens to the frequency channel's status for x ms before packet transmission. Based on computer simulation results, CSMA-x can reduce the packet collision rate. Moreover, a Markov model-based theoretical performance analysis of LBT in LoRaWAN was performed

in [15], where LBT- and ALOHA-based nodes coexist. Based on theoretical analysis, packet delivery rates improve with an increase in the ratio of LBT nodes in the network. However, the LBT protocol increases the node's energy consumption as the node must check the frequency channel [31]. In addition, the hidden node problem may occur with a high probability in LPWAN because of the significant coverage area [16]. The hidden node problem occurs when a node fails CS and accesses a busy frequency channel. The probability of CS success depends on the CS threshold of the node and LPWAN nodes generally have poor CS thresholds.

In [28], we proposed a frequency channel and transmission timing allocation scheme in event-triggered traffic. The scheme prevented packet collisions when event-triggered traffic was based on Q-learning. Each node autonomously selects its transmission timing and frequency channel by introducing a Q-learning mechanism at every node and experiencing event-triggered traffic. However, a learning duration and learning processing on the node side is required.

An algorithm called MIX-MAB, in which each node determines resource allocation in a decentralized manner, is proposed in [32]. MIX-MAB solves the resource allocation problem by modeling a multi-armed bandit in reinforcement learning. MIX-MAB achieves fast convergence speed and higher PDR compared with conventional LoRa. However, the performance of MIX-MAB is significantly influenced by the number of nodes and DC because MIX-MAB requires ACK as a reward in reinforcement learning.

An autonomous decentralized control, such as LBT has no overheads of the control signal. LBT operates without severe harmful effects from clock drift because the transmission timing is determined based on the CS. However, in LPWAN with a large communication area, packet collisions owing to the hidden node problem occur frequently. In addition, the communication quality is generally inferior to that of the centralized control system because less information is available for resource control than in the centralized control system.

B. Objective and Main Contributions of This Study

As previously mentioned, packet collision avoidance is vital in LPWANs with *periodic traffic*. Therefore, our objective is to avoid periodic or continuous packet collisions. A fundamental premise of conventional methods is to eliminate the effect of clock drift through synchronization because clock drift causes unintentional changes in the transmission timing. However, we overturned the premise of synchronization and proposed a resource allocation scheme utilizing clock drift for packet collision avoidance in a fully asynchronous system.

Although centralized scheduling schemes, such as SMAC [19] effectively avoid packet collisions, scheduling overhead cannot be ignored, including broadcast beacon. In addition, synchronization in periodic traffic may adversely influence the system's performance. Suppose two nodes are synchronized and their initial transmission timing offsets and transmission periods match. In that case, packet collision always occurs, significantly degrading the nodes' packet delivery rate (PDR) performance. Avoiding such constant packet collisions by

sending a control signal is challenging because the GW cannot observe the nodes with constant packet collisions. Furthermore, the scheduling scheme must compensate for clock drift to improve the PDR of the entire system. In other words, periodic traffic is always faced with a dilemma because synchronization and scheduling improve the overall PDR but may significantly degrade the PDR of particular nodes. Generally, clock drift is considered harmful to the system. However, a clear utilization of clock drift can avoid continuous packet collisions in periodic traffic. Therefore, this study proposes an adaptive resource allocation scheme that utilizes clock drift, which is generally considered to be harmful. Once a GW receives a data packet, the GW predicts packet collisions based on the packet transmission period of each node and the packet reception time. The GW then allocates the transmission offset time and frequency channel using DL packets to avoid predicted packet collisions. In addition, a simple clock drift compensation is applied. The GW estimates the clock drift of each node by comparing its receive timing with its transmission period and the GW can calculate the compensation value from the estimated clock drift. Continuous packet collision can be avoided by considering the clock drift during transmission timing offset decision. Clock drift occurs based on probability because of temperature and other factors. Therefore, completely compensating for clock drift is challenging, resulting in residual clock drift. This residual clock drift may cause unpredictable and continuous packet collisions among particular nodes. We introduce a packet discard probability for each node to reduce the impact of such unpredictable continuous packet collisions. By discarding packets based on probability, continuous packet collisions become intermittent, enabling the GW to recognize the nodes in which packet collisions occur.

Based on computer simulation results, the proposed scheme can improve the PDR by 25% and 22% compared with the pure ALOHA protocol and SMAC-based protocol [19], respectively, in the LoRaWAN environment [33]. Furthermore, we prove that sequential clock drift compensation and packet discard probability can reduce the number of nodes with a severely degraded PDR performance.

The main contributions of this study are as follows.

- (i) A centralized control type resource allocation scheme for periodic traffic is proposed. The proposed scheme efficiently avoids packet collisions by utilizing clock drift, which is generally harmful.
- (ii) Simple clock drift compensation is performed by allocating resources to nodes without transmitting control signals for synchronization. Simple clock drift compensation enables transmission timing control based on the periodicity of packet transmission.
- (iii) Because full compensation of clock drift is challenging and residual clock drift exists, unpredictable packet collisions occur. Therefore, this study introduces a packet discard probability to reduce the effect of residual clock drift.

C. Organization

The remainder of this paper is structured as follows. The LoRaWAN-based system model is described in Section II,

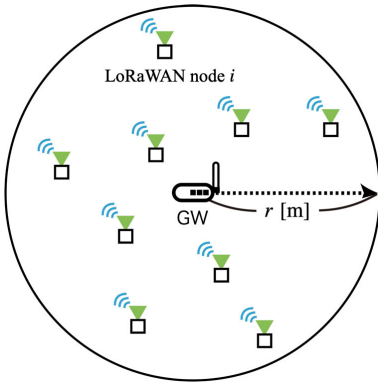


Fig. 1. System model.

TABLE I
SNR AND SIR THRESHOLDS [37], [38]

| SF S | SNR threshold $\Gamma^{\text{SNR}}(S)$ [dB] | SIR threshold $\Gamma^{\text{SIR}}(S)$ [dB] |
|--------|---|---|
| 7 | -7.5 | -11 |
| 8 | -10 | -13 |
| 9 | -12.5 | -16 |
| 10 | -15 | -19 |
| 11 | -17.5 | -22 |
| 12 | -20 | -24 |

including the clock drift and channel models. Section III explains the proposed adaptive resource allocation scheme that utilizes clock drift and packet discard probability. Section IV provides computer simulation results. Finally, the conclusions of the study are provided in Section V.

II. SYSTEM MODEL

This study follows the LoRaWAN-based system model, the most widely investigated among LPWAN technology. The physical layer of the LoRaWAN is called *LoRa modulation*, which is based on frequency shift chirp modulation (FSCM). FSCM is a combination of chirp spread spectrum (CSS) [34] modulation and frequency-shift keying [35]. LoRa modulation achieves a high level of interference tolerance by transmitting narrow-band signals spread over a system bandwidth [36].

A. Network Model

The network model has a star topology that comprises I LoRaWAN nodes (set $\mathcal{I} = \{1, \dots, i, \dots, I\}$) and one GW. The nodes are uniformly and randomly distributed in a circular communication area of radius r [m] centered on the GW, as shown in Fig.1. Each node selects an K orthogonal frequency channel (set $\mathcal{K} = \{1, \dots, k, \dots, K\}$) for packet transmission. The nodes and GW transmit data packets as unconfirmed messages that do not require an acknowledgement (ACK) from the receiver.

B. Data Packet

LoRa modulation has a key parameter called SF, which influences communication performance. SF is set to a value between 7 and 12 (set $\mathcal{S} = \{7, 8, \dots, 12\}$), and determines the number of bits transmitted by one CSS symbol [39]. When

node i selects SF $S_i \in \mathcal{S}$, the length of one CSS symbol $T_i^s(S_i)$ [s] is expressed as:

$$T_i^s(S_i) = 2^{S_i}/W, \quad (1)$$

where W [Hz] is the frequency bandwidth.

The LoRaWAN packet comprises a preamble, synchronization word, physical header, header cyclic redundancy check (CRC), physical payload, and payload CRC [40]. The required number of CSS symbols to transmit one LoRaWAN packet is expressed as [35]

$$N_i^s(S_i) = O_{\text{sym}} + \left\lceil \frac{B_{\text{data}}/R_{\text{code}}}{S_i} \right\rceil, \quad (2)$$

where $\lceil x \rceil$ is the ceiling function of x , O_{sym} is the number of symbols required for transmission in addition to the physical payload and CRC, B_{data} [bit] is the data size of the physical payload and CRC, and R_{code} is the coding rate. Thus, the time-on-air (ToA) of one data packet, $T_i^{\text{ToA}}(S_i)$ [sec], is expressed as:

$$T_i^{\text{ToA}}(S_i) = T_i^s(S_i) \times N_i^s(S_i). \quad (3)$$

The signal-to-noise power ratio (SNR) $\Gamma^{\text{SNR}}(S)$ and signal-to-interference power ratio (SIR) thresholds $\Gamma^{\text{SIR}}(S)$ for each SF are listed in Table I. SNR threshold Γ^{SNR} required for successful packet reception decreased as SF increased [37]. Packet collision occurred when multiple packets arrived at the receiver simultaneously. Generally, the LoRaWAN system operates asynchronously; thus, the reception timings of multiple packets differ. In such a situation, the receiver synchronizes with the packet arriving first. The receiver then attempts to demodulate the received signal through the de-chirping and DFT operations. The receiver determines the transmitted symbol by searching the maximum peak of the DFT output. Suppose the input signal has a sufficiently higher SIR relative to the interfering signal. In that case, the receiver can select the correct peak and determine the transmitted symbol. That is, a capture effect works [38]. The capture effect in LoRaWAN occurs in the following two scenarios [41]. First, the occurrence of packet collision between nodes using the same SF. Here, suppose the SIR of the first-arriving signal at the GW is greater than the SIR threshold of 6 [dB]. In that case, reception succeeds owing to the capture effect. Second, the occurrence of packet collision between nodes that use different SFs. Here, the capture effect succeeds provided the SIR of the first-arriving signal at the GW is above the SIR threshold of each SF shown in Table I.

C. Transmitting Node

We considered a class A node, a mandatory feature of a node in the LoRaWAN system. We assumed periodic UL traffic, emulating environmental monitoring and other applications [17], [18]. Each node generated UL packets with a data size of B_{data} [bit]. Node i generated UL packets by following the UL packet generation cycle G_i^p [min], randomly determined when the node is placed in the communication area. Notably, G_i^p is fixed after it is determined and is expressed as:

$$G_i^p \sim \mathcal{U}(1, G_{\text{max}}^p), \quad (4)$$

where G_{\max}^p [min] is the maximum UL packet generation cycle, function $\mathcal{U}(1, G_{\max}^p)$ generates a uniform random integer number ranging from $[1, G_{\max}^p]$. The first packet generation time of node i , T_i^{FP} , is expressed as:

$$T_i^{\text{FP}} \sim \mathcal{U}'(0, G_{\max}^p), \quad (5)$$

where $\mathcal{U}'(0, G_{\max}^p)$ is a uniform random number generated in the order of ms ranging from $[0, G_{\max}^p]$. Thus, node i generated packets with a fixed cycle G_i^p from time T_i^{FP} . Node i transmitted the generated UL packet to the GW using frequency channel $k_i \in \mathcal{K}$ and SF $S_i \in \mathcal{S}$. Here, SF S_i was allocated based on the SNR value at the GW [37].

Each node always satisfied the DC constraint because the UL packet generation cycle was large relative to the DC constraint. Notably, all UL packets were transmitted as unconfirmed packets.

After a node completes the transmission of UL packets, it opens one receive window after waiting for W_d [s] [40]. Here, W_d , which is the same for all nodes, is the waiting time between the node finishing the transmission of UL packets and the opening of the receiving window. This study assumes that DL packets are successfully received provided they are transmitted from the GW when the reception window of node i is open.

D. GW

Because class A nodes were considered, the GW must transmit a DL packet while the node opens a receiving window [40]. When a DL packet to node i is generated, the GW transmits the DL packet using the same SF S_i on frequency channel K_i , same as node i .

The GW stopped DL packet generation on a particular frequency channel once the DL packet was transmitted to guarantee the DC constraint. The waiting time, $T_{k_i}^{\text{DC}}$, required to satisfy DC after DL packet transmission to node i is expressed as:

$$T_{k_i}^{\text{DC}} = \left(\frac{1 - D_c}{D_c} \right) T_i^{\text{ToA}}(S_i) \quad (6)$$

where $D_c \in (0, 1]$ is the DC.

Because half-duplex communication was adopted, the overlap between UL packet reception and DL packet transmission at the GW should be considered. This study prioritized a UL packet more than a DL packet. Thus, two cases are described below.

- Case 1: The transmission of a DL packet is timed while the GW is receiving a UL packet. In this case, the GW discards the DL packet because the node can receive the DL packet only when its receiving window is open.
- Case 2: A UL packet arrives at the GW while the GW is transmitting a DL packet. In this case, the GW cannot receive the UL packet.

Notably, the GW can simultaneously receive multiple UL packets on different frequency channels as long as the GW is not transmitting a DL packet.

E. Clock Drift Model

Clock drift is defined as the relative time shift between the GW and each node. At node i , clock drift occurs following

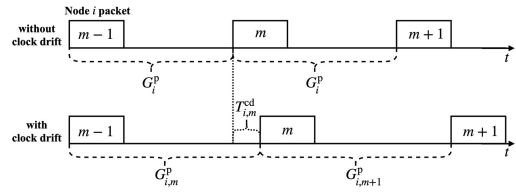


Fig. 2. Effect of clock drift on periodic traffic.

a node-specific normalized clock drift of ΔT_i^{cd} . At time t , normalized clock drift $\Delta T_i^{\text{cd}}(t)$ of node i is randomly determined following a Gaussian distribution $\mathcal{N}(\mu_i, \sigma_i^2)$ with mean μ_i and variance σ_i^2 [11]. Thus, the clock drift of node i , $T_{i,m}^{\text{cd}}$, that occurs between the $(m-1)$ th and m th UL packet generation cycles is expressed as:

$$T_{i,m}^{\text{cd}} = \int_{(m-1) \times G_i^p}^{m \times G_i^p} \Delta T_i^{\text{cd}}(t) dt. \quad (7)$$

As shown in Fig. 2, the UL packet generation cycle of node i changes owing to clock drift $T_{i,m}^{\text{cd}}$. Therefore, the m th UL packet generation cycle, $G_{i,m}^p$, becomes

$$G_{i,m}^p = G_i^p + T_{i,m}^{\text{cd}}. \quad (8)$$

F. Channel Model

Without loss of generality, the channel model only includes path loss because we aim to evaluate the impact of traffic control on communication quality. The received signal power of node i is expressed as:

$$P_i^r = P_t - P_{\text{Loss}}(d_i), \quad (9)$$

where P_t [dBm] is the transmit power common to the nodes and a GW, and $P_{\text{Loss}}(d_i)$ [dB] is the path loss component, where d_i [km] is the physical distance from the GW to node i . The path loss model assumes a non-line-of-sight (NLoS) environment in urban areas. From [42], the path loss component $P_{\text{Loss}}(d_i)$ [dB] is expressed as:

$$P_{\text{Loss}}(d_i) = 10\alpha \log_{10} d_i + \beta + 10\eta \log_{10} f_c, \quad (10)$$

where the propagation parameters α , β , and η are the path loss coefficient, offset, and frequency loss component, respectively, and f_c [MHz] is the carrier frequency. We assume that the UL and DL channel profiles between node i and the GW are reciprocal; hence, the received signal power from the GW at node i is assumed to be equal to P_i^r . The SNR $\gamma_{\text{SNR},i}$ [dB] and SIR $\gamma_{\text{SIR},i}$ [dB] of the transmitted signal of node i at the GW are expressed as:

$$\begin{cases} \gamma_{\text{SNR},i} &= P_i^r - (N_0 + 10 \log_{10} W + NF) \\ \gamma_{\text{SIR},i} &= P_i^r - \sum_{i' \in \mathcal{I}_i} P_{i'}^r, \end{cases} \quad (11)$$

where N_0 [dBm/Hz] is the noise power spectrum density, NF [dB] is the noise figure, and \mathcal{I}_i is the set of interfering nodes in the system that simultaneously transmit packets on the same frequency channel as node i . The GW would succeed in receiving the UL packet provided $\gamma_{\text{SNR},i}$ and $\gamma_{\text{SIR},i}$ exceed the SNR and SIR thresholds shown in Table I, respectively.

III. PROPOSED SCHEME

This section explains the proposed resource allocation scheme that utilizes periodic traffic and clock drift for continuous packet collision avoidance.

In TDMA, a typical packet collision avoidance scheme, different time slots are assigned to different nodes. However, the TDMA-based approach has numerous limitations. First, all the nodes in the system must be synchronized. Thus, a synchronization signal from the GW must be transmitted to the nodes. This is challenging for nodes that cannot receive a DL signal at any arbitrary time. Furthermore, the synchronization may misalign with time, owing to the clock drift. Second, a combinatorial optimization problem should be solved for optimal time slot allocation. However, solving a combinatorial optimization problem in LoRaWAN where many nodes exist is challenging.

Thus, this study proposes a centralized resource allocation scheme comprising *clock drift compensation*, *frequency channel allocation*, and *transmission timing offset allocation* to overcome these challenges; however, the scheme does not require any synchronization among nodes. The clock drift compensation can exploit a secondary effect of clock drift (continuous packet collision avoidance). Note that we cannot *perfectly* compensate for clock drift in advance because it does not occur deterministically. Thus, residual clock drift exists regardless of whether we compensate for clock drift. Therefore, the proposed scheme allocates a frequency channel and transmission timing offset, considering the effect of residual clock drift. Table II lists the main notation and definitions used in this section.

A. Flow of the Proposed Scheme

The main flow of the proposed scheme is explained here. The GW is supposed to receive UL packets periodically from each node. Thus, the GW can estimate the node's UL packet generation cycle if the GW successfully receives packets from a node multiple times. The estimated UL packet generation cycle is used to estimate the clock drift of each node and predict each node's UL packet transmission timing. Therefore, the GW can predict packet collisions by comparing the estimated transmission timing of each node. The general flow of the proposed scheme is as follows.

- (i) Estimation of UL packet generation cycle G_i^p : The GW estimates each node's UL packet generation cycle based on the reception time of UL packets.
- (ii) Clock drift estimation: The GW calculates the clock drift compensation value $\hat{T}_i^{\text{cd}\star}$ for node i based on the estimated UL packet generation cycle.
- (iii) Packet collision prediction: The GW calculates whether a packet collision occurs from the timing of each node's packet transmission.
- (iv) Transmission timing offset candidate calculation: Suppose the GW predicts packet collisions in the subsequent packet transmission. In that case, the GW calculates a transmission timing offset candidate to avoid predicted packet collisions.
- (v) Frequency channel and transmission timing offset determination: The GW determines frequency channel

k_i^* and transmission timing offset $T_i^{\text{off}\star}$ for node i that can considerably avoid packet collisions.

- (vi) Parameter allocation through the DL channel: The GW generates a DL packet containing the allocation control information for clock drift compensation value $\hat{T}_i^{\text{cd}\star}$, new frequency channel k_i^* , and transmission timing offset $T_i^{\text{off}\star}$, as well as transmits the packet to the node. Hereinafter, we focus on a particular node and omit node index i for simplicity, unless otherwise necessary.

1) *Estimation of the UL Packet Generation Cycle*: Each packet contains a frame counter. Once the GW receives packets more than twice from a particular node, the GW can estimate the UL packet generation cycle G^p from the frame counter and reception timings. Let $n(j)$ and $T(j)$ denote the frame counter (FCntUp) and reception timing of the j th successfully received packet from the node, respectively. Hence, the GW estimates packet generation cycle \hat{G}^p [min] as

$$\hat{G}^p = G_{\min}^p \times \text{round}\left(\frac{T(j) - T(j-1)}{G_{\min}^p \times (n(j) - n(j-1))}\right), \quad (12)$$

where G_{\min}^p is the minimum unit of the UL packet generation cycle and $\text{round}(x)$ is a function rounded to the nearest integer value. Once GW successfully receives more than one packet from the node, we assume the GW can ideally estimate the UL packet generation cycle G^p , first packet generation time T^{FP} , and packet ToA T^{ToA} .

2) *Clock Drift Estimation and Compensation*: The GW can observe the clock drift value T_j^{cd} that occurred between the reception of the $(j-1)$ th and j th packets of the node. Upon the reception of the j th packet from the node, the GW calculates the normalized clock drift as follows:

$$\Delta \hat{T}_j^{\text{cd}} = \frac{T(j) - T(j-1)}{G^p \times (n(j) - n(j-1))}, \quad (13)$$

Thus, the estimated normalized clock drift $\Delta \hat{T}^{\text{cd}}$ is obtained as:

$$\Delta \hat{T}^{\text{cd}} = \frac{1}{j} \sum_{j'=1}^j \Delta \hat{T}_{j'}^{\text{cd}}. \quad (14)$$

The clock drift cannot be changed by a control signal from the GW because it is determined by the physical properties of node circuits. However, the GW can adjust each node's UL packet generation cycle by sending a control signal. Therefore, we compensate for the clock drift by changing the UL packet generation cycle G^p of the node. The GW calculates $\hat{T}^{\text{cd}\star}$ to compensate for the change in G_j^p owing to clock drift, such that the UL packet generation cycle can be adjusted to the original G^p . The clock drift compensation value $\hat{T}^{\text{cd}\star}$ is expressed as:

$$\hat{T}^{\text{cd}\star} = \frac{G^p \Delta \hat{T}^{\text{cd}}}{1 + \Delta \hat{T}^{\text{cd}}}. \quad (15)$$

As shown in Fig.3, the node-allocated clock drift compensation value $\hat{T}^{\text{cd}\star}$ changed its UL packet generation cycle to $G^p - \hat{T}^{\text{cd}\star}$. Thus, the UL packet generation cycle with clock drift can be shortened to correct UL packet generation cycle G^p as follows:

$$G_m^p \simeq G^p - \hat{T}^{\text{cd}\star} + \int_0^{(G^p - \hat{T}^{\text{cd}\star})} \Delta T^{\text{cd}}(t) dt. \quad (16)$$

TABLE II
SUMMARY OF MAIN NOTATIONS IN SECTION III

| | |
|-----------------------|---|
| $\hat{T}_i^{cd\star}$ | Clock drift compensation value for node i |
| k_i^\star | Frequency channel to be allocated for node i |
| T^{off} | Transmission timing offset already allotted to node i |
| $T_i^{off\star}$ | Transmission timing offset to be allocated for node i |
| $n(j)$ | FCntUp of the j th successfully received packet |
| $T(j)$ | Reception timing of the j th successfully received packet |
| G^P | Packet generation cycle estimated by GW |
| T_j^{cd} | Clock drift value observed at GW when the j th packet successfully received |
| $\Delta\hat{T}^{cd}$ | Estimated normalized clock drift |
| T^{pred} | Packet collision prediction period |
| F | Number of packets to be predicted |
| f | Predicted number of packets index of F |
| $g_k(\cdot)$ | Packet collision count function at frequency channel k |
| \mathcal{T}_k^e | Set of packet transmission end timing of other nodes allocated to frequency channel k |
| $\mathcal{T}_k^e(i')$ | i' th element of set \mathcal{T}_k^e |
| \mathcal{T}_k^{off} | Set of candidate offsets in frequency channel k |
| \mathbf{P} | Packet discard probability matrix |
| p_i | Packet discard probability of node i |

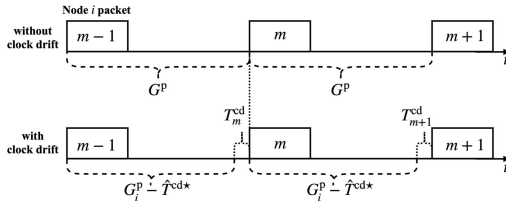


Fig. 3. Example of clock drift compensation.

Because clock drift occurs based on probability, perfectly compensating for clock drift at all nodes is challenging, and residual clock drift may be maintained.

3) *Packet Collision Prediction*: Suppose the GW knows node's UL packet generation cycle G^P . In that case, the GW can estimate reception timing $\hat{T}(n(j) + 1)$ of the $(n(j) + 1)$ th packet based on the UL packet generation cycle of the node and the j th packet reception timing, $T(j)$. Similarly, $\hat{T}(n(j) + 2)$ can be calculated from G^P and $\hat{T}(n(j) + 1)$. Furthermore, the GW can estimate the packet transmission duration of the node from $\hat{T}(n(j) + 1)$ and the ToA of the node. Thus, the GW compares the estimated packet transmission durations of each node. Suppose the estimated packet transmission durations overlap on the same frequency channel. In that case, the GW would predict the occurrence of packet collisions. Therefore, after receiving the j th packet from the node, the GW estimates the scheduled packet transmission time of all the nodes during the packet collision prediction period T^{pred} from the packet reception time $T(j)$. The estimated packet transmission time for a clock drift-compensated node is based on the assumption that the clock drift is perfectly compensated for. However, the estimated clock drift values are utilized to calculate UL packet generation cycle G^P for nodes that have not yet compensated for the clock drift but consider the clock drift. The packet collision prediction period, T^{pred} , for the node is defined as follows:

$$T^{pred} = G^P \times (F + 1) - T^{ToA}, \quad (17)$$

where F denotes the number of packets to be predicted.

After receiving packets from the node, the GW checks whether its transmission time overlaps with those of other nodes in each frequency channel during the packet collision prediction period T^{pred} . We assume a counting function $g_k(T^{off})$ checks the number of collisions during T^{pred} provided T^{off} is to be allocated to the node on frequency channel k . Suppose $g_{k^\star}(T^{off}) = 0$ on the currently allocated frequency, k^\star . In that case, no further processing is performed for the node. Otherwise, the GW would calculate transmission timing offset candidates in the next step.

4) *Transmission Timing Offset Candidate Calculation*: Let \mathcal{T}_k^e denote the set of packet transmission end timing of other nodes allocated to frequency channel k during T^{pred} in ascending order. Algorithm 1 was used to calculate transmission timing offset candidates. The GW calculated a transmission timing offset by comparing the start time of the $(n(j) + f)$ th packet from the node to the transmission completion time of other nodes as follows:

$$\mathcal{T}_k^e(i') - T_{n(j)+f}^G + T^{off} > T^{ToA} + \left| G^P \Delta\hat{T}^{cd} \right|, \quad (18)$$

for $0 \leq i' < |\mathcal{T}_k^e|$

where $\mathcal{T}_k^e(i')$ denotes the i' th element of set \mathcal{T}_k^e . Suppose (18) is satisfied. In that case, the temporary transmission timing offset T_{temp}^{off} is obtained as follows:

$$T_{temp}^{off} = \left(\mathcal{T}_k^e(i') - T_{n(j)+f}^G + T^{off} + \frac{G^P \Delta\hat{T}^{cd}}{2} \right) \bmod G^P, \quad (19)$$

where $G^P \Delta\hat{T}^{cd}$ is divided by 2 to have a guard time before and after the packet transmission time to absorb the residual clock drift. Suppose the proposed algorithm runs continuously. In that case, the transmission offset time T_i^{off} may exceed that of the UL packet generation cycle G_i^P . Therefore, by adopting modular arithmetic, as shown in Eq. (19), the transmission offset time T_i^{off} can be shifted to the same position in units within the UL packet generation cycle G_i^P , as shown in Fig.4.

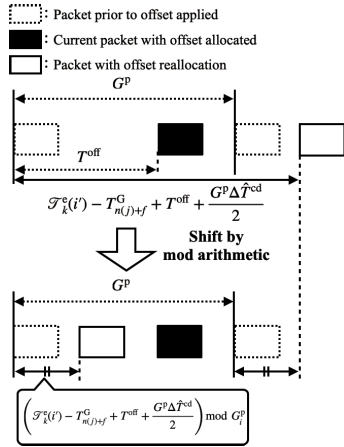


Fig. 4. Offset time modification by modular arithmetic.

5) Frequency Channels and Transmission Timing Offset

Determination: The GW allocated a frequency channel k^* and transmission timing offset $T^{\text{off}*}$ to the node. The GW would terminate the allocation for the node when $\mathcal{T}_k^{\text{off}} = \emptyset, \forall k$. In a WSN, the delay between data generation at the node and its arrival at the information aggregation station should be considerably small. Thus, the exploration policy of set \mathcal{T}^{off} is to minimize the transmission timing offset while considerably avoiding packet collisions. The GW selects the following frequency channel and transmission offset time:

$$\begin{aligned} k^* &= \operatorname{argmin}_{0 \leq k < K} T_k^{\min}, \\ T^{\text{off}*} &= \min_{0 \leq k < K} T_k^{\min}, \end{aligned} \quad (20)$$

where $T_k^{\min} = \min_{t \in \mathcal{T}_k^{\text{off}}} t$. Eq. (20) calculates the offset candidate with the minimum offset from $\{\mathcal{T}_0^{\text{off}}, \dots, \mathcal{T}_k^{\text{off}}, \dots, \mathcal{T}_{K-1}^{\text{off}}\}$ obtained from Algorithm 1. Thus, k^* and $T^{\text{off}*}$ are determined simultaneously.

Algorithm 1 Algorithm to Calculate the Transmission Offset Time Candidate

```

1: Input:
2:    $\mathcal{T}_k^e, T^{\text{off}}$ 
3: Initialization:
4:    $\mathcal{T}_k^{\text{off}} = \emptyset, \forall k$ 
5: for  $k = 1 \dots K$  do
6:   for  $f = 1 \dots F$  do
7:     for  $i' = 1 \dots |\mathcal{T}_k^e|$  do
8:       if  $\mathcal{T}_k^e(i') - T_{n(j)+f}^G + T^{\text{off}} > T^{\text{ToA}} + \left| G^P \Delta \hat{T}^{\text{cd}} \right|$  then
9:          $T^{\text{tmp}} = \left( \mathcal{T}_k^e(i') - T_{n(j)+f}^G + T^{\text{off}} + \frac{G^P \Delta \hat{T}^{\text{cd}}}{2} \right) \bmod G^P$ 
10:        if  $g_k(T^{\text{tmp}}) = 0$  then
11:           $\mathcal{T}_k^{\text{off}} = \mathcal{T}_k^{\text{off}} \cup T^{\text{tmp}}$ 
12:          Break
13:        end if
14:      end if
15:    end for
16:  end for
17: end for
18: Output:
19:    $\mathcal{T}_0^{\text{off}}, \dots, \mathcal{T}_k^{\text{off}}, \dots, \mathcal{T}_{K-1}^{\text{off}}$ 

```

6) **Parameter Allocation:** The proposed scheme used DL packets to allocate the clock drift compensation value $\hat{T}^{\text{cd}*}$,

frequency channel k^* , and transmit timing offset $T^{\text{off}*}$ to the node. For power saving, each LoRaWAN node is mandated to open a DL receive window for a predetermined time only after the transmission of UL packets. Generally, the DL receive window opens 1 s after the UL packet transmission ends, regardless of the packet message type. Thus, the GW can transmit DL packets as it knows the opening time of the node's DL receive window. However, from Section II-D, the GW cannot transmit DL packets continuously because of the DC constraint on DL packet transmission. Therefore, to efficiently improve the PDR of the entire system, DL packets are only transmitted to the nodes that satisfy at least one of the following conditions.

- Condition 1: The number of packet losses increases compared with the previous packet reception. The GW can detect the packet loss of a particular node based on the packet reception time, FCntUp, and UL packet generation cycle.
- Condition 2: The residual clock drift is larger than 1 [ms] owing to imperfect clock drift compensation. The GW can detect the residual clock drift based on the packet reception cycle of the node.

B. Setting Packet Discard Probability

Perfectly compensating for clock drift at all the nodes is challenging because the clock drift changes based on probability, owing to a node's circuit and other factors; hence, residual clock drift is maintained at some nodes. Although the transmission timing shift owing to residual clock drift is considerably smaller than that owing to clock drift itself, it may result in packet collisions. Residual clock drift may cause continuous packet collisions provided a node has the same transmission period or an integer multiple of the transmission period of the other node. This is because the transmission timing shift by residual clock drift is slight compared with packet ToA. Therefore, the overlap occurred owing to residual clock drift; it is challenging to solve. Because such packet loss owing to residual clock drift is unpredictable, it cannot be overcome using any deterministic approach. Thus, this study introduced a probabilistic packet transmission. Accordingly, the GW could receive data packets from some nodes even in the case of residual clock drift. A node with long ToA or short packet generation cycle may result in severe continuous packet collisions. Conversely, a node with short ToA or long packet generation cycles is not likely to cause continuous packet collisions. However, packet loss resulting from packet discard may be more severe. Therefore, this study allocates packet discard probability to nodes based on their ToA and packet generation cycle. The packet discard probability matrix, \mathbf{P} , is expressed as:

$$\mathbf{P} = \alpha f(\mathbf{s} \otimes \mathbf{c}^T), \quad (21)$$

where $\alpha \in [0, 1)$ is the predetermined maximum packet discard probability and \mathbf{s} is the ToA candidate vector. \mathbf{c} is the transmission cycle vector normalized by the maximum UL packet generation cycle, \otimes is the Kronecker product operator, \top is the transpose operator, and $f(\mathbf{X})$ denotes the function that normalizes all components of the matrix \mathbf{X} using the maximum value of \mathbf{X} . Node i selects the component of the

TABLE III
SIMULATION PARAMETERS

| | |
|--------------------------------------|--|
| Simulation area radius, r | 895 [m] |
| Simulation time | 3000 [min] |
| Number of LoRaWAN nodes, I | {250, 500, 750, 1000, 1250} |
| Transmit power, P_t | 13 [dBm] |
| Carrier frequency, f_c | 0.923 [GHz] |
| Bandwidth, W | 125 [kHz] |
| Number of frequency channels, K | {1, 2, 4, 8, 16} |
| SF, S | {7, 8, 9, 10} |
| Coding rate, R_{code} | 4/7 |
| Duty cycle, D_c | 0.01 |
| Noise power spectrum density, N_0 | -174 [dBm/Hz] |
| Noise figure, NF | 10 [dB] |
| Path loss coefficient, α | 4.0 |
| Propagation offset, η | 9.5 |
| Frequency loss component, ξ | 4.5 |
| Overhead symbol, O_{sym} | 20.25 |
| Packet data size, B_{data} | 160 [bits] |
| G_{max}^p | 10 [min] |
| F | 3 |
| $\{\mu_{min}, \mu_{max}\}$ | $\{-1.91 \times 10^{-3}, 0.28 \times 10^{-3}\}$ |
| $\{\sigma_{min}^2, \sigma_{max}^2\}$ | $\{9.59 \times 10^{-11}, 3.19 \times 10^{-10}\}$ |
| α | 0.1 |

packet discard probability matrix \mathbf{P} corresponding to T_i^{ToA} and G_i^p as packet discard probability p_i .

IV. SIMULATION AND RESULTS

A. Parameter Set

The simulation parameters are listed in Table III. The LoRaWAN system parameters follow the Japanese parameter configuration AS923 [40]. The maximum SF was 10 and a single packet's ToA was limited to 400 [ms]. LoRaWAN nodes were placed randomly and uniformly within a communication area of radius $r = 895$ [m], where $r = 895$ [m] was the maximum communication distance with an SF of 10 under the channel model considered. Without loss of generality, we assumed all LoRaWAN nodes transmitted data packets of the same data size with the number of overhead symbols $B_{data} = 160$ [bits] and $O_{sym} = 20.25$.

Each LoRaWAN node randomly selected its UL packet cycles from $1 \sim 10$ [min]. μ_i and σ_i^2 , which determine the normalized clock drift ΔT_i^d of node i , were randomly determined from the range $[\mu_{min}, \mu_{max}]$, $[\sigma_{min}^2, \sigma_{max}^2]$, which were experimentally obtained [11]. Retransmission is not performed because the nodes transmit a data packet as an unconfirmed message.

B. Evaluation Criteria

This study adopted the PDR, total system throughput, and packet reception cycle (PRC) as performance metrics.

1) *Packet Delivery Rate*: This study treated packets canceled owing to the packet discard probability as lost packets. The PDR must be evaluated for a particular observation period owing to periodic traffic. Thus, we defined the maximum UL packet generation cycle as an observation

period indexed by c ($\{1, \dots, c, \dots, C\}$). The PDR during the c th observation period is calculated as follows:

$$\text{PDR}_c \triangleq \frac{\sum_{i=1}^I N_{i,c}^{\text{succ}}}{\sum_{i=1}^I N_{i,c}^{\text{tran}}}, \quad (22)$$

where $N_{i,c}^{\text{succ}}$ is the number of UL packets of node i successfully received by the GW during the c th observation period and $N_{i,c}^{\text{tran}}$ is the total number of packets transmitted by node i during the c th observation period.

Furthermore, we evaluated the PDR of each LoRaWAN node, expressed as:

$$\text{PDR}_i \triangleq \frac{\sum_{c=1}^C N_{i,c}^{\text{succ}}}{\sum_{c=1}^C N_{i,c}^{\text{tran}}}. \quad (23)$$

2) *Throughput*: The throughput of node i , R_i [bps] is defined as:

$$R_i \triangleq \text{PDR}_i \times \frac{B_{data}}{T_i^{\text{ToA}}(S_i)}. \quad (24)$$

Thus, the total system throughput, R [bps], is defined as:

$$R \triangleq \sum_{i=1}^I R_i. \quad (25)$$

3) *Packet Reception Cycle*: We calculated the normalized packet reception cycle (PRC) to evaluate the impact of continuous packet collisions. The normalized PRC of node i is defined as:

$$\text{PRC}_i \triangleq \frac{1}{J_i - 1} \sum_{j=1}^{J_i} \left(\frac{T_{i,j}^R - T_{i,j-1}^R}{G_i^p} \right), \quad (26)$$

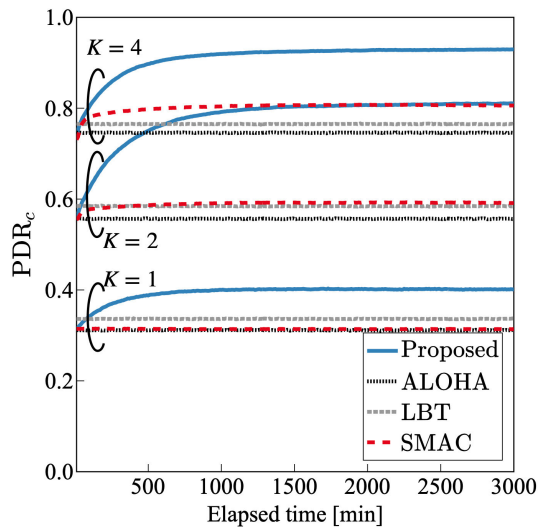
where J_i is the number of UL packets of node i successfully received at the GW and $T_{i,j}^R$ [sec] is the reception time of the j th packet at the GW. Thus, PRC_i became 1 when the GW periodically received the packets without loss.

C. Benchmark Methods

This study adopted pure ALOHA and SMAC as benchmark methods to evaluate the effectiveness of the proposed scheme.

1) *Pure ALOHA Protocol*: In ALOHA, each LoRaWAN node transmitted a UL packet upon its generation by randomly selecting a frequency channel; that is, frequency hopping was applied [40].

2) *LBT Protocol*: LBT Protocol: The LBT is another benchmark method proposed by [30] that is less complex than CSMA/CA and can be easily implemented in LoRaWAN. In LBT, the node i performed CS for the CS period $T^{\text{CS}} = 5$ [msec] at frequency channel k_i once it generated a UL packet. Assuming the CS threshold is defined as $\Gamma^{\text{CS}} = -110$ [dBm]. Suppose no signal is detected from other nodes in the CS period T^{CS} . In that case, the node would transmit the UL packet immediately after the CS ends. However, the node would wait for a transmission using binary backoff upon completion of the CS period provided the node detects a signal from another node. After the backoff time elapses, the node performed CS again. This process was repeated until the number of CS repetitions n_r reached 6 for a single UL packet. When the

Fig. 5. PDR_c for $I = 1000$.

number of CS repetitions is n_r , the backoff time T_{back}^{CS} [msec] is determined as

$$T_{back}^{CS} = \mathcal{U}(0, 2^{n_{min}^{CS} + n_r}), \quad (27)$$

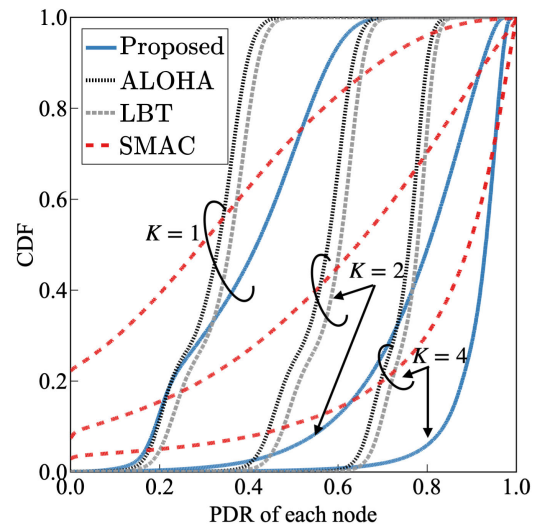
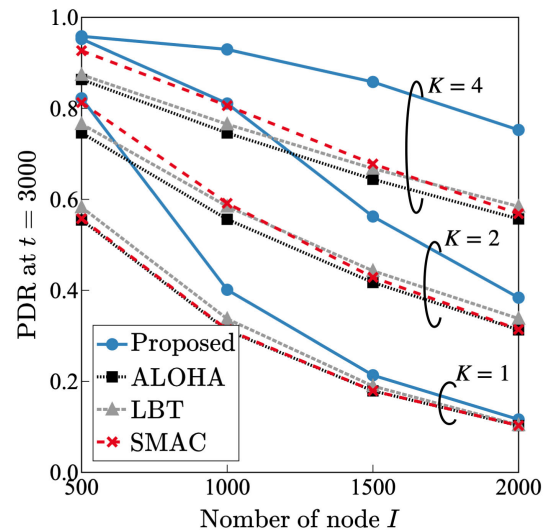
where $n_{min}^{CS} = 7$ is the minimum backoff exponent.

3) *SMAC-Based Protocol*: SMAC is another benchmark method proposed for periodic traffic [19]. Although the SMAC protocol assumes orthogonality between different SFs [19], different SFs interfere [38], [43]. Thus, this study compared the SMAC with a modified version that considered the non-orthogonality between different SFs. SMAC allocated only frequency channels that can avoid packet collisions based on the packet generation cycle and the transmission timing of each node. Following [19], we assumed a *perfectly synchronized system, void of clock drift*.

D. Results

1) *PDR Performance*: The PDR_c performance with $I = 1000$ nodes is shown in Fig. 5, according to which the proposed scheme improves the PDR performance with time, irrespective of the number of frequency channels K . This is because the number of nodes allocated to a transmission offset and frequency channel that could avoid packet collisions using the proposed scheme increased. The proposed scheme improved the PDR performance by approximately 25%, 23%, and 22% compared with the pure ALOHA, LBT, and SMAC-based protocols, respectively, for $K = 2$. The performance of the SMAC-based protocol was almost identical to that of pure ALOHA protocol for $K = 1$ because it only allocated frequency channels. The SMAC-based protocol improved the PDR performance compared with the pure ALOHA protocol owing to packet collision avoidance as the number of frequency channels increased.

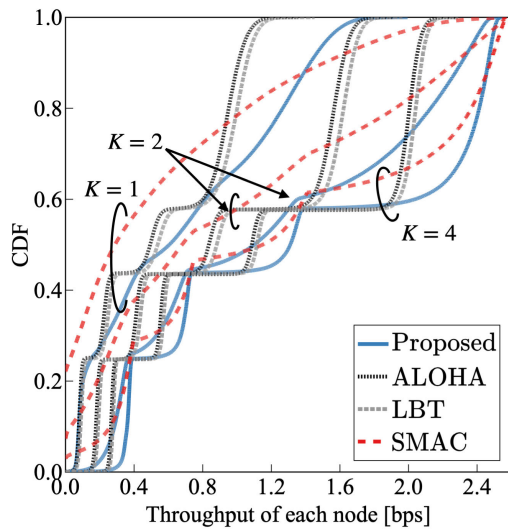
The cumulative distribution function (CDF) of each node's PDR performance is shown in Fig. 6, according to which the proposed scheme could shift the curves in the right direction and bring up their tail. Therefore, the proposed scheme can perform packet collision avoidance without impairing

Fig. 6. CDF of the PDR per node for $I = 1000$.Fig. 7. Impact of the PDR per number of nodes at $c = 30$.

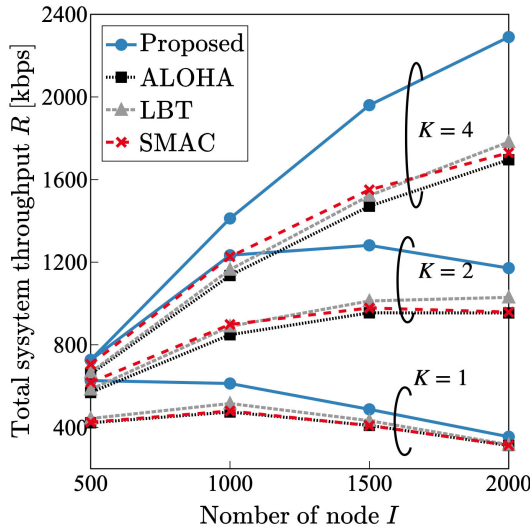
fairness among nodes. However, the proposed scheme slightly increased the ratio of the low PDR performance compared with ALOHA and LBT. This is because the proposed scheme performed semi-synchronization with clock drift compensation, resulting in continuous packet collisions among particular nodes.

Owing to the synchronous operation of SMAC-based protocol, continuous packet collisions may occur depending on the UL packet generation cycle, initial transmission timing, and initial frequency channel. Thus, as shown in Fig. 6, some nodes have PDR_i of 0. However, *the proposed scheme prevented continuous packet collisions by utilizing transmission-timing deviations owing to clock drift*. Further, the packet discard probability suppressed the occurrence of continuous packet collisions caused by semi-synchronization owing to clock drift compensation.

The PDR_c at an observation period of $c = 30$ as a function of the number of nodes is shown in Fig. 7. The proposed scheme improved the PDR performance compared with the pure ALOHA, LBT, and SMAC-based protocols, irrespective



(a) CDF of the throughput per node for $I = 1000$



(b) Total system throughput R

Fig. 8. Throughput performance.

of the number of frequency channels and nodes, as shown in Fig. 7. When the number of frequency channels was $K = 1$, the proposed scheme performed packet collision avoidance using only the transmit offset. Therefore, when the number of nodes is small, the proposed scheme can improve the PDR performance compared with the pure ALOHA protocol. In addition, when the number of frequency channels was $K = 4$, the proposed scheme utilized a combination of frequency channels and transmit offsets to avoid packet collisions, thus improving the PDR performance compared with the pure ALOHA protocol even with an increased number of nodes. When the number of nodes increased, SMAC achieved a lower PDR than LBT. This is because SMAC, which is a centralized control method, cannot transmit control signals to some nodes owing to DC constraints and cannot allocate the appropriate frequency channels. However, the proposed scheme achieved a better PDR than LBT for all numbers of nodes despite the centralized control method.

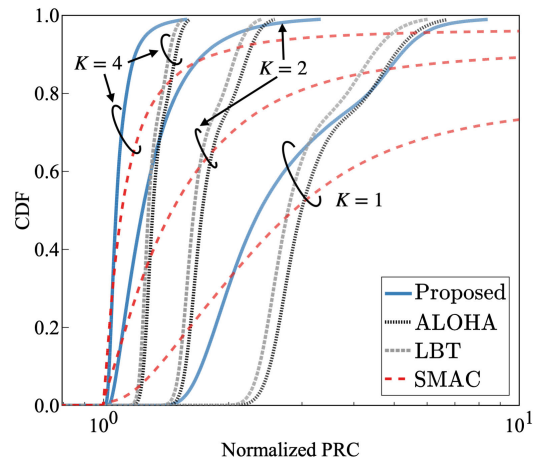


Fig. 9. CDF of the PRC for $I = 1000$.

2) *Throughput Performance*: The CDF of the throughput of each node R_i when the number of nodes is $I = 1000$ is shown in Fig. 8(a). The CDF curves became a series of steps as the number of frequency channels K increased. This is because the PDR performance increased with an increasing number of channels. Thus, the effect of the data rate per SF became visible.

Based on the figure, the proposed scheme increased the ratio of nodes with high throughput compared with the benchmark methods, irrespective of the number of frequency channels. In addition, although the proposed scheme allocated a higher packet discard probability to nodes with higher SF, the CDF performance was improved compared with that of the benchmark methods, even in regions of low throughput ($S = 10$). Therefore, the packet discard probability did not significantly degrade the throughput of some nodes.

As shown in Fig. 8(b), the proposed scheme improved the total system throughput R compared with the benchmark methods irrespective of the number of nodes and frequency channels.

3) *PRC Performance*: The CDF of PRC_i with the number of nodes $I = 1000$ is shown in Fig. 9, according to which the proposed scheme has a better PRC performance compared with the pure ALOHA protocol, irrespective of the number of frequency channels. This is because although the proposed scheme incurred a transmission delay owing to the transmission offset, it can effectively ensure the successful reception of packets by the GW owing to packet collision avoidance. In the proposed scheme, when the number of frequency channels decreased, the number of nodes with large PRC increased. This is because the transmission offset allocated to each node increased for packet collision avoidance. The proposed scheme decreased the ratio of the number of nodes with a large PRC compared with the SMAC-based protocol because the SMAC-based protocol was prone to continuous packet collisions owing to the synchronous system, whereas the proposed scheme avoided continuous packet collisions by utilizing the shift resulting from clock drift.

V. CONCLUSION

This study focused on periodic traffic in WSNs and proposed an adaptive resource allocation scheme that utilized clock drift. In the proposed scheme, the GW predicted future packet collision based on the periodic traffic feature and determined the transmission offset and frequency channel for each node. Subsequently, each node performed transmission timing and frequency channel allocation after quasi-synchronization through clock drift compensation. Furthermore, based on probability, each node discarded a packet to avoid continuous packet collisions owing to quasi-synchronization. Based on numerical results, the proposed scheme improved the PDR performance by approximately 25% and 22% compared with the pure ALOHA and SMAC-based protocols, respectively.

Therefore, clock drift is effective in avoiding packet collisions in periodic traffic. Thus, we believe that low overhead packet collision avoidance is possible provided clock drift can be effectively utilized in autonomous distributed resource allocation. The proposed scheme provided packet collision avoidance in asynchronous systems. Consequently, the energy consumption of the nodes could be saved compared with synchronous systems, which require the reception of control signals for synchronization.

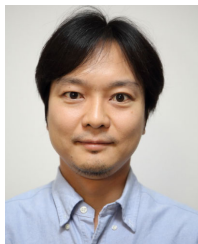
REFERENCES

- [1] A. Zanella, N. Bui, A. Castellani, L. Vangelista, and M. Zorzi, "Internet of Things for smart cities," *IEEE Internet Things J.*, vol. 1, no. 1, pp. 22–32, Feb. 2014.
- [2] M. Jouhari, N. Saeed, M.-S. Alouini, and E. Mehdi Amhoud, "A survey on scalable LoRaWAN for massive IoT: Recent advances, potentials, and challenges," 2022, *arXiv:2202.11082*.
- [3] O. Georgiou and U. Raza, "Low power wide area network analysis: Can LoRA scale?" *IEEE Wireless Commun. Lett.*, vol. 6, no. 2, pp. 162–165, Apr. 2017.
- [4] W. Guibene, J. Nowack, N. Chalikias, K. Fitzgibbon, M. Kelly, and D. Prendergast, "Evaluation of LPWAN technologies for smart cities: River monitoring use-case," in *Proc. IEEE Wireless Commun. Netw. Conf. Workshops (WCNCW)*, Mar. 2017, pp. 1–5.
- [5] U. Raza, P. Kulkarni, and M. Sooriyabandara, "Low power wide area networks: An overview," *IEEE Commun. Surveys Tuts.*, vol. 19, no. 2, pp. 855–873, 2nd Quart., 2017.
- [6] M. Ballerini, T. Polonelli, D. Brunelli, M. Magno, and L. Benini, "NB-IoT versus LoRaWAN: An experimental evaluation for industrial applications," *IEEE Trans. Ind. Informat.*, vol. 16, no. 12, pp. 7802–7811, Dec. 2020.
- [7] R. Marini, K. Mikhaylov, G. Pasolini, and C. Buratti, "Low-power wide-area networks: Comparison of LoRaWAN and NB-IoT performance," *IEEE Internet Things J.*, vol. 9, no. 21, pp. 21051–21063, Nov. 2022.
- [8] Z. Qin, F. Y. Li, G. Y. Li, J. A. McCann, and Q. Ni, "Low-power wide-area networks for sustainable IoT," *IEEE Wireless Commun.*, vol. 26, no. 3, pp. 140–145, Jun. 2019.
- [9] S. Popli, R. K. Jha, and S. Jain, "A survey on energy efficient narrowband Internet of Things (NB-IoT): Architecture, application and challenges," *IEEE Access*, vol. 7, pp. 16739–16776, 2019.
- [10] D. Djenouri and M. Bagaa, "Synchronization protocols and implementation issues in wireless sensor networks: A review," *IEEE Syst. J.*, vol. 10, no. 2, pp. 617–627, Jun. 2016.
- [11] K. Tsurumi, A. Kaburaki, K. Adachi, O. Takyu, M. Ohta, and T. Fujii, "Simple clock drift estimation and compensation for packet-level index modulation and its implementation in LoRaWAN," *IEEE Internet Things J.*, vol. 9, no. 16, pp. 15089–15099, Aug. 2022.
- [12] J. Haxhibeqiri, I. Moerman, and J. Hoebeke, "Low overhead scheduling of LoRA transmissions for improved scalability," *IEEE Internet Things J.*, vol. 6, no. 2, pp. 3097–3109, Apr. 2019.
- [13] L. Tassarò, C. Raffaldi, M. Rossi, and D. Brunelli, "Lightweight synchronization algorithm with self-calibration for industrial LoRA sensor networks," in *Proc. Workshop Metrology for Ind. 4.0 IoT*, Apr. 2018, pp. 259–263.
- [14] C. Garrido-Hidalgo et al., "LoRaWAN scheduling: From concept to implementation," *IEEE Internet Things J.*, vol. 8, no. 16, pp. 12919–12933, Aug. 2021.
- [15] J. Ortín, M. Cesana, and A. Redondi, "Augmenting LoRaWAN performance with listen before talk," *IEEE Trans. Wireless Commun.*, vol. 18, no. 6, pp. 3113–3128, Jun. 2019.
- [16] L. Beltramelli, A. Mahmood, P. Österberg, and M. Gidlund, "LoRa beyond ALOHA: An investigation of alternative random access protocols," *IEEE Trans. Ind. Informat.*, vol. 17, no. 5, pp. 3544–3554, May 2021.
- [17] R. K. Verma, S. Bharti, and K. K. Pattanaik, "GDA: Gravitational data aggregation mechanism for periodic wireless sensor networks," in *Proc. IEEE SENSORS*, Oct. 2018, pp. 1–4.
- [18] V. Gupta, S. K. Devar, N. H. Kumar, and K. P. Bagadi, "Modelling of IoT traffic and its impact on LoRaWAN," in *Proc. IEEE Global Commun. Conf.*, Dec. 2017, pp. 1–6.
- [19] Z. Xu, J. Luo, Z. Yin, T. He, and F. Dong, "S-MAC: Achieving high scalability via adaptive scheduling in LPWAN," in *Proc. IEEE Conf. Comput. Commun.*, Jul. 2020, pp. 506–515.
- [20] K. Mikhaylov, P. Masek, T. Hanninen, M. Stusek, and J. Hosek, "Improving LoRaWAN performance by randomizing network access for data and on-air activation," in *Proc. IEEE Int. Conf. Commun.*, May 2022, pp. 4432–4437.
- [21] A. H. Nguyen, Y. Tanigawa, and H. Tode, "Scheduling method for solving successive contentions of heterogeneous periodic flows based on mathematical formulation in multi-hop WSNs," *IEEE Sensors J.*, vol. 18, no. 21, pp. 9021–9033, Nov. 2018.
- [22] S. Kaul, M. Gruteser, V. Rai, and J. Kenney, "Minimizing age of information in vehicular networks," in *Proc. 8th Annu. IEEE Commun. Soc. Conf. Sensor, Mesh Ad Hoc Commun. Netw.*, Jun. 2011, pp. 350–358.
- [23] S. Kaul, R. Yates, and M. Gruteser, "Real-time status: How often should one update?" in *Proc. IEEE INFOCOM*, Mar. 2012, pp. 2731–2735.
- [24] M. Moltafet, M. Leinonen, and M. Codreanu, "Worst case age of information in wireless sensor networks: A multi-access channel," *IEEE Wireless Commun. Lett.*, vol. 9, no. 3, pp. 321–325, Mar. 2020.
- [25] R. D. Yates and S. K. Kaul, "The age of information: Real-time status updating by multiple sources," *IEEE Trans. Inf. Theory*, vol. 65, no. 3, pp. 1807–1827, Mar. 2019.
- [26] A. Kaburaki, K. Adachi, O. Takyu, M. Ohta, and T. Fujii, "Resource allocation for periodic traffic in wireless sensor network," in *Proc. IEEE Wireless Commun. Netw. Conf. (WCNC)*, Mar. 2023, pp. 1–6.
- [27] Z. Qin and J. A. McCann, "Resource efficiency in low-power wide-area networks for IoT applications," in *Proc. IEEE Global Commun. Conf.*, Dec. 2017, pp. 1–7.
- [28] A. Kaburaki, K. Adachi, O. Takyu, M. Ohta, and T. Fujii, "Autonomous decentralized traffic control using Q-learning in LPWAN," *IEEE Access*, vol. 9, pp. 93651–93661, 2021.
- [29] S. U. Minhaj et al., "Intelligent resource allocation in LoRaWAN using machine learning techniques," *IEEE Access*, vol. 11, pp. 10092–10106, 2023.
- [30] T.-H. To and A. Duda, "Simulation of LoRA in NS-3: Improving LoRA performance with CSMA," in *Proc. IEEE Int. Conf. Commun. (ICC)*, May 2018, pp. 1–7.
- [31] Z. Xie, R. Xu, and L. Lei, "A study of clear channel assessment performance for low power wide area networks," in *Proc. 10th Int. Conf. Wireless Commun., Netw. Mobile Comput. (WiCOM)*, Sep. 2014, pp. 311–315.
- [32] F. Azizi, B. Teymuri, R. Aslani, M. Rasti, J. Tolvaneny, and P. H. J. Nardelli, "MIX-MAB: Reinforcement learning-based resource allocation algorithm for LoRaWAN," in *Proc. IEEE 95th Veh. Technol. Conf. (VTC-Spring)*, Jun. 2022, pp. 1–6.
- [33] *LoRaWAN L2 1.0.4 Specification*, document TS001-1.0.4, Oct. 2020.
- [34] A. Springer, W. Gugler, M. Huemer, L. Reindl, C. C. W. Ruppel, and R. Weigel, "Spread spectrum communications using chirp signals," in *Proc. IEEE/AFCEA EUROCOMM Inf. Syst. Enhanced Public Saf. Secur.*, 2000, pp. 166–170.
- [35] L. Vangelista, "Frequency shift chirp modulation: The LoRA modulation," *IEEE Signal Process. Lett.*, vol. 24, no. 12, pp. 1818–1821, Dec. 2017.
- [36] B. Reynders, W. Meert, and S. Pollin, "Range and coexistence analysis of long range unlicensed communication," in *Proc. 23rd Int. Conf. Telecommun. (ICT)*, May 2016, pp. 1–6.

- [37] Semtech. *Semtech SX1272 Datasheets*. Accessed: May 8, 2023. [online]. Available: <https://www.semtech.com/products/wireless-RF/loracore/sx1272>
- [38] D. Croce, M. Gucciardo, S. Mangione, G. Santaromita, and I. Tinnirello, "Impact of LoRa imperfect orthogonality: Analysis of link-level performance," *IEEE Commun. Lett.*, vol. 22, no. 4, pp. 796–799, Apr. 2018.
- [39] D. Bankov, E. Khorov, and A. Lyakhov, "On the limits of LoRaWAN channel access," in *Proc. Int. Conf. Eng. Telecommun. (EnT)*, Nov. 2016, pp. 10–14.
- [40] LoRa Alliance. (Dec. 2018). *LoRaWAN Regional Parameters v1.1rB*. [Online]. Available: https://loralliance.org/sites/default/files/2018-04/lorawantm_regional_parameters_v1.1rb_-_final.pdf
- [41] A. Waret, M. Kaneko, A. Guitton, and N. El Rachkidy, "LoRa throughput analysis with imperfect spreading factor orthogonality," *IEEE Wireless Commun. Lett.*, vol. 8, no. 2, pp. 408–411, Apr. 2019.
- [42] P. Series. (2017). *Propagation Data and Prediction Methods for the Planning of Short-Range Outdoor Radiocommunication Systems and Radio Local Area Networks in the Frequency Range 300 MHz to 100 GHz*. [Online]. Available: <https://www.itu.int/rec/R-REC-P.1411-9-201706-S/en>
- [43] B. Reynders and S. Pollin, "Chirp spread spectrum as a modulation technique for long range communication," in *Proc. Symp. Commun. Veh. Technol. (SCVT)*, Nov. 2016, pp. 1–5.



Aoto Kaburaki (Graduate Student Member, IEEE) received the B.E. and M.E. degrees in information and communication engineering from The University of Electro-Communications, Japan, in 2020 and 2022, respectively, where he is currently pursuing the Ph.D. degree. His research interests include machine learning and its application to wireless communication.



Koichi Adachi (Senior Member, IEEE) received the B.E., M.E., and Ph.D. degrees in engineering from Keio University, Japan, in 2005, 2007, and 2009, respectively.

From 2007 to 2010, he was a Research Fellow at the Japan Society for the Promotion of Science (JSPS). He was a Visiting Researcher at the City University of Hong Kong, Hong Kong, in April 2009, and a Visiting Research Fellow at the University of Kent, U.K., from June 2009 to August 2009. From May 2010 to May 2016, he was with the Institute for Infocomm Research, A*STAR, Singapore. He is currently an Associate Professor with The University of Electro-Communications, Japan. His research interests include cooperative communication and energy-efficient communication technologies.

Dr. Adachi is a member of IEICE. He was awarded an Excellent Editor Award from IEEE ComSoc MMTC in 2013. He is the coauthor of the WPMC 2020 Best Student Paper Award. He served as the General Co-Chair for the 10th and 11th IEEE Vehicular Technology Society Asia Pacific Wireless Communications Symposium (APWCS); the Track Co-Chair for the Transmission Technologies and Communication Theory of the 78th and 80th IEEE Vehicular Technology Conference in 2013 and 2014, respectively; the Symposium Co-Chair for the Communication Theory Symposium of the IEEE GLOBECOM 2018 and the Wireless Communications Symposium of the IEEE GLOBECOM 2020; and the Tutorial Co-Chair for the IEEE ICC 2019. He was an Associate Editor of *IET Transactions on Communications* from 2015 to 2017, IEEE WIRELESS COMMUNICATIONS LETTERS since 2016, IEEE TRANSACTIONS ON VEHICULAR TECHNOLOGY from 2016 to 2018, IEEE TRANSACTIONS ON GREEN COMMUNICATIONS AND NETWORKING since 2016, and IEEE OPEN JOURNAL OF VEHICULAR TECHNOLOGY since 2019. He was recognized as an Exemplary Reviewer of the IEEE WIRELESS COMMUNICATIONS LETTERS in 2012, 2013, 2014, and 2015.



Osamu Takyu (Member, IEEE) received the B.E. degree in electrical engineering from the Tokyo University of Science, Chiba, Japan, in 2002, and the M.E. and Ph.D. degrees in open and environmental systems from Keio University, Yokohama, Japan, in 2003 and 2006, respectively. From 2003 to 2007, he was a Research Associate at the Department of Information and Computer Science, Keio University. From 2004 to 2005, he was a Visiting Scholar at the School of Electrical and Information Engineering, The University of Sydney. From 2007 to 2011, he was an Assistant Professor with the Department of Electrical Engineering, Tokyo University of Science. From 2011 to 2013, he was an Assistant Professor with the Department of Electrical and Computer Engineering, Shinshu University, where he was an Associate Professor from 2013 to 2023, and has been a Professor since 2023. His current research interests include wireless communication systems and distributed wireless communication technology. He was a recipient of the Young Researcher's Award of IEICE 2010, the 2010 Active Research Award in radio communication systems from the IEICE Technical Committee on RCS, and the 2018 Best Paper Award in Smart Radio from IEICE technical committee on SR.



Mai Ohta (Member, IEEE) received the B.E., M.E., and Ph.D. degrees in electrical engineering from The University of Electro-Communications, Tokyo, Japan, in 2008, 2010, and 2013, respectively.

Since 2013, she has been an Assistant Professor at the Department of Electronics Engineering and Computer Science, Fukuoka University. Her research interests include cognitive radio, spectrum sensing, LPWAN, and sensor networks.

Dr. Ohta was a recipient of the Young Researcher's Award from IEICE in 2013.



Takeo Fujii (Senior Member, IEEE) received the B.E., M.E., and Ph.D. degrees in electrical engineering from Keio University, Yokohama, Japan, in 1997, 1999, and 2002, respectively.

From 2000 to 2002, he was a Research Associate with the Department of Information and Computer Science, Keio University. From 2002 to 2006, he was an Assistant Professor with the Department of Electrical and Electronic Engineering, Tokyo University of Agriculture and Technology. From 2006 to 2014, he was an Associate Professor with the Advanced Wireless and Communication Research Center, The University of Electro-Communications, where he is currently a Professor and the Director. His current research interests include cognitive radio and ad-hoc wireless networks.

Dr. Fujii is a fellow of IEICE. He was a recipient of the Best Paper Award from the IEEE VTC 1999-Fall, the 2001 Active Research Award in radio communication systems from the IEICE Technical Committee of RCS, the 2001 Ericsson Young Scientist Award, the Young Researcher's Award from the IEICE in 2004, the Young Researcher Study Encouragement Award from the IEICE Technical Committee of AN in 2009, the Best Paper Award from IEEE CCNC 2013, and the IEICE Communication Society Best Paper Award in 2016.